Plasma Astrophysics

Toshiki Tajima, UCI

Class 7:PHY249 (2020Spring)

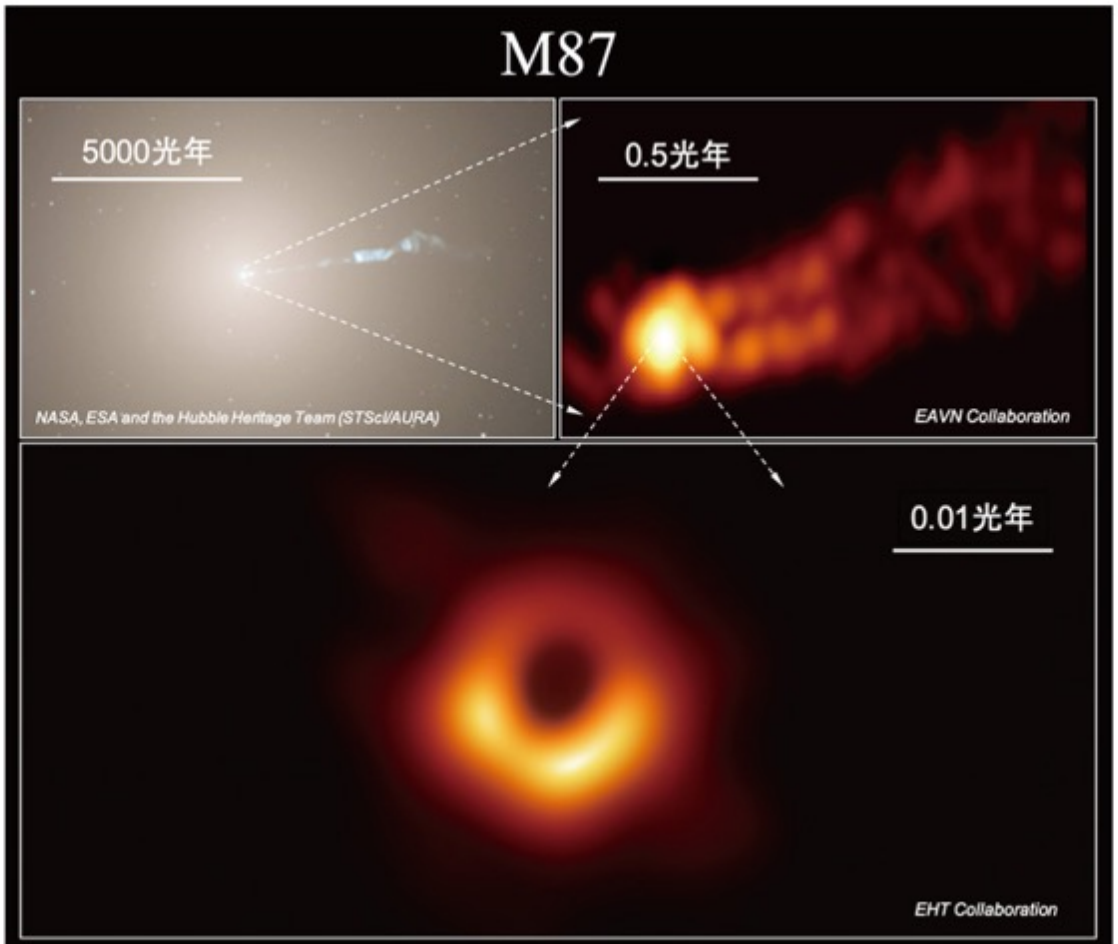

Event Horizon Telescope (2020)

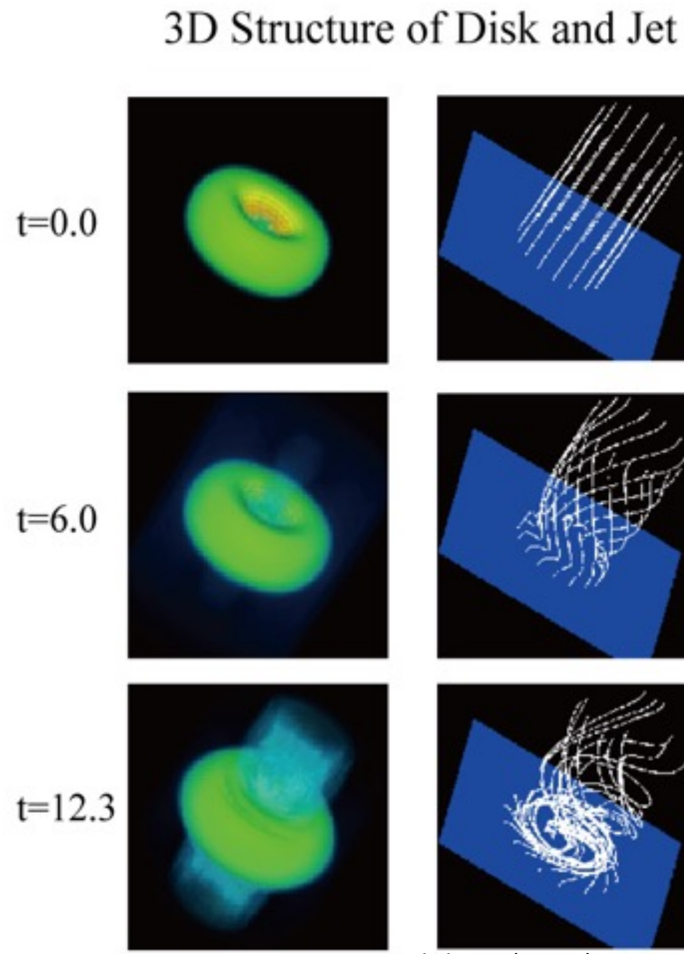

Tajima Shibata (1997) p. 387

Plasma Astrophysics (Tajima, 2020)

- Class 7:Term Project Buildup

Localizable Brightest cosmic rays by wakefields ?

(A)

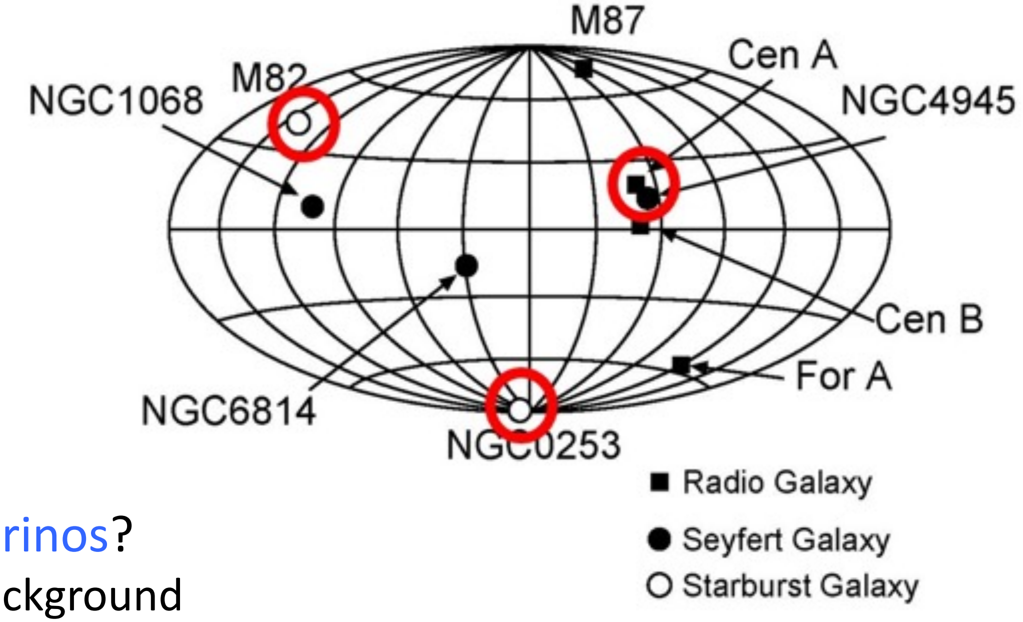

Localized UHECR?

thus Localized neutrinos?

not as a spread background

(B)

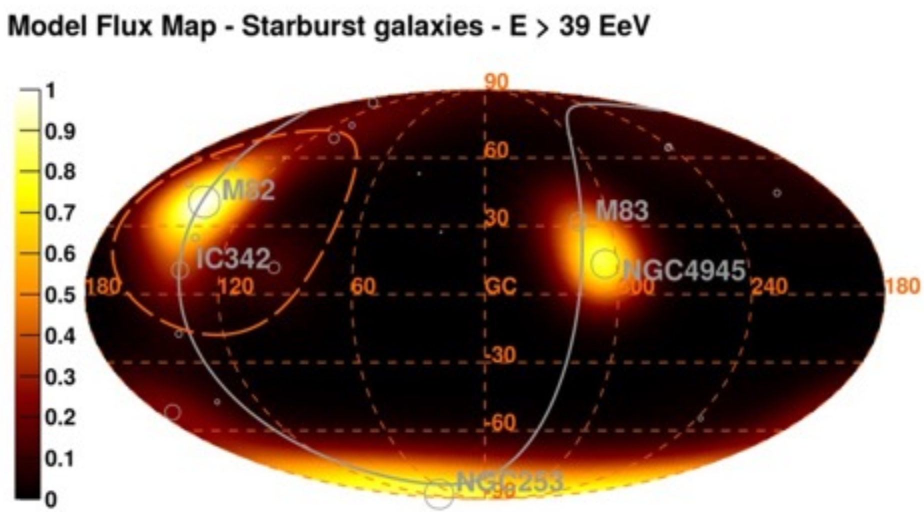

cosmic ray acceleration and gamma-ray emission

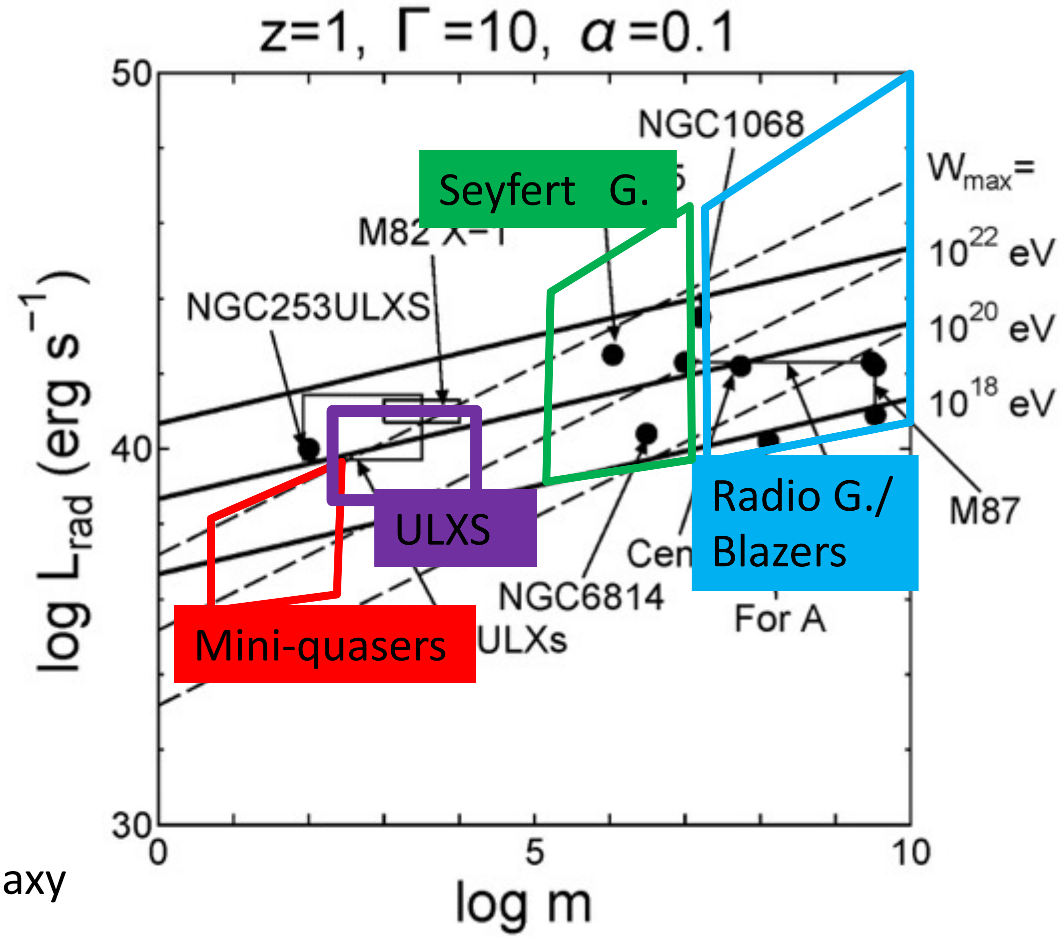

Miniquasars:
can be in our Galaxy

Ebisuzaki, Tajima
EPJ **223**, 1113(2014); (2020)

BH Astronomy with Ultra High Energy CRs

Term Project structure

I. Contrast : **characteristics** of the prevailing theory
←→ new theory

II. Examples of **new phenomena** explainable
by new theory

III. **Generalized jet** characteristics

IV. Emerging new view of the Universe

I. Contrast of old vs. new

Prevailing theory (Fermi's stochastic acceleration; 1954)

a. energy beyond 10^{19} eV not possible

b. isotropic HECR arrival

c. No time structure

d. No expected other signals s.a. γ emissions

New Theory (Wakefield acceleration; 1979-)

not to deny the old theory, but can explain new things

A. beyond $10^{18\text{-}19}$ eV possible

B. localized

C. time structured

D. correlated with other signals (s.a. γ emissions, etc.)

E. non-protons (s.a. pinpointed neutrino)

Fermi stochastic acceleration

Incoherent stochastic process requires <u>bending</u>→synchrotron loss

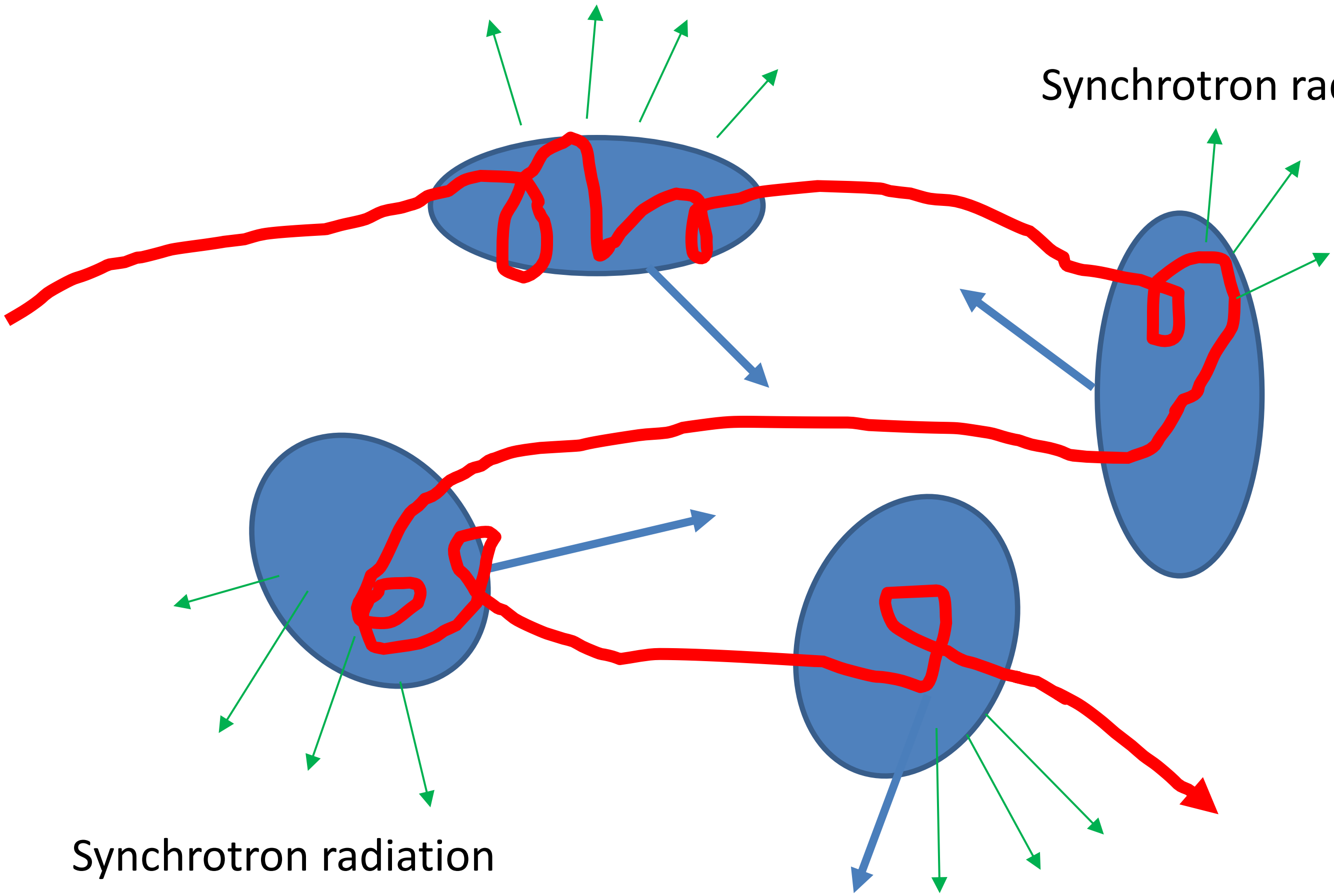

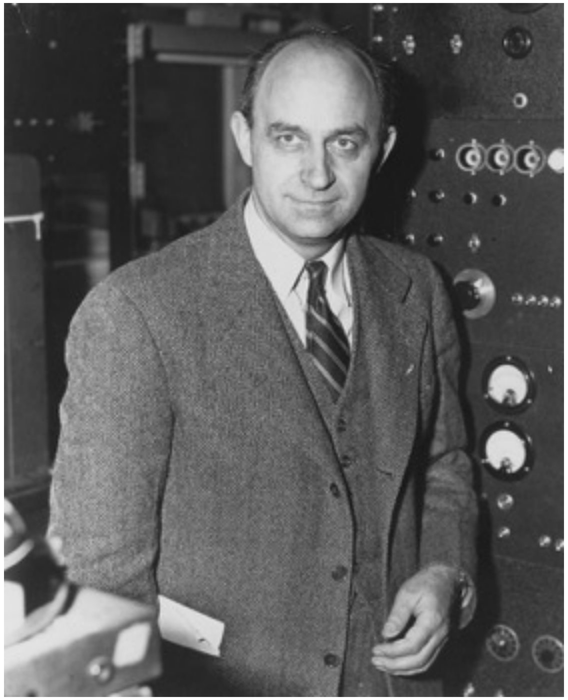

Enrico Fermi
By Department of Energy. Office of Public Affairs

E. Fermi, ApJ **119** (1954) 1.

Wakefields: Bow and Wake

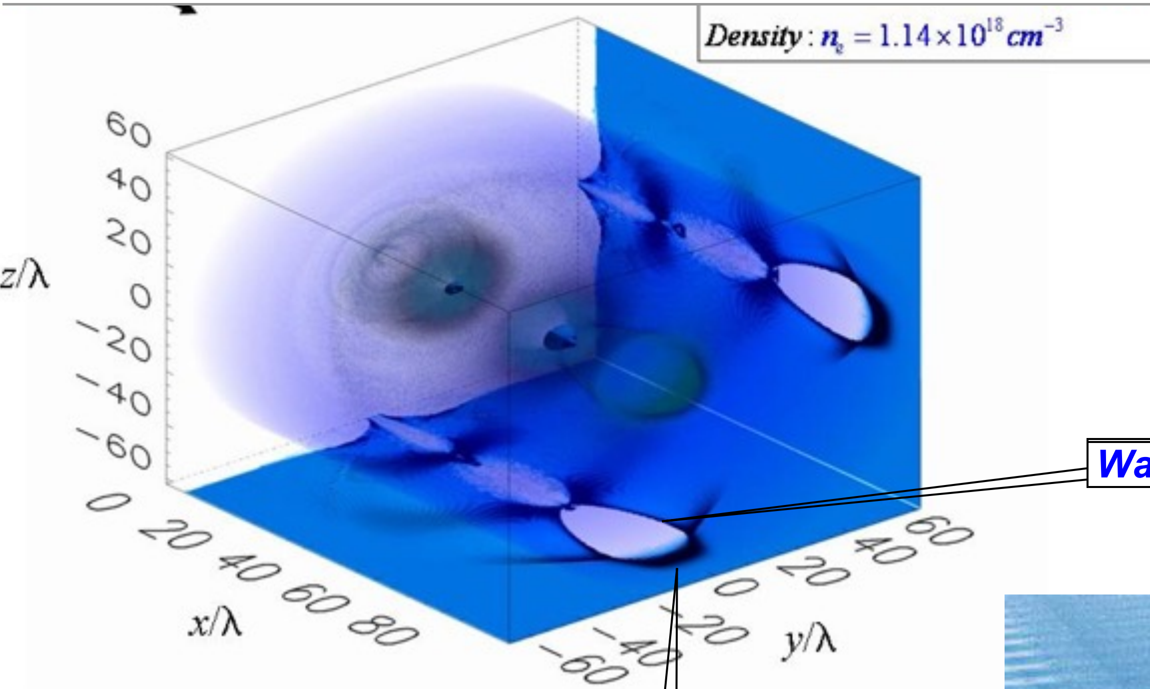

(Bulanov, Esirkepov)

Wakefield acceleration

Wake Wave

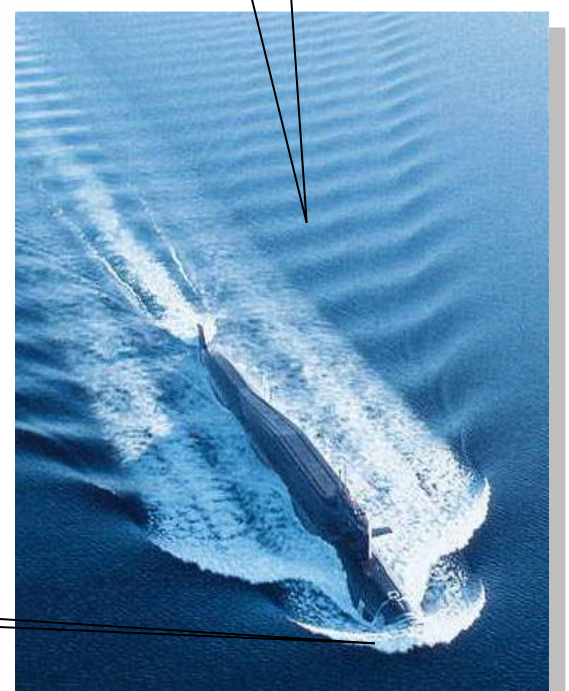

Coherent, collective,
robust, huge amplitude

Bow Wave

Ponderomotive acceleration

Universal Theory of Wakefield toward extreme energy

$$\Delta E \approx 2 m_0 c^2 a_0^2 \gamma_{ph}^2 = 2 m_0 c^2 a_0^2 \left(\frac{n_{cr}}{n_e} \right),$$ (when 1D theory applies)

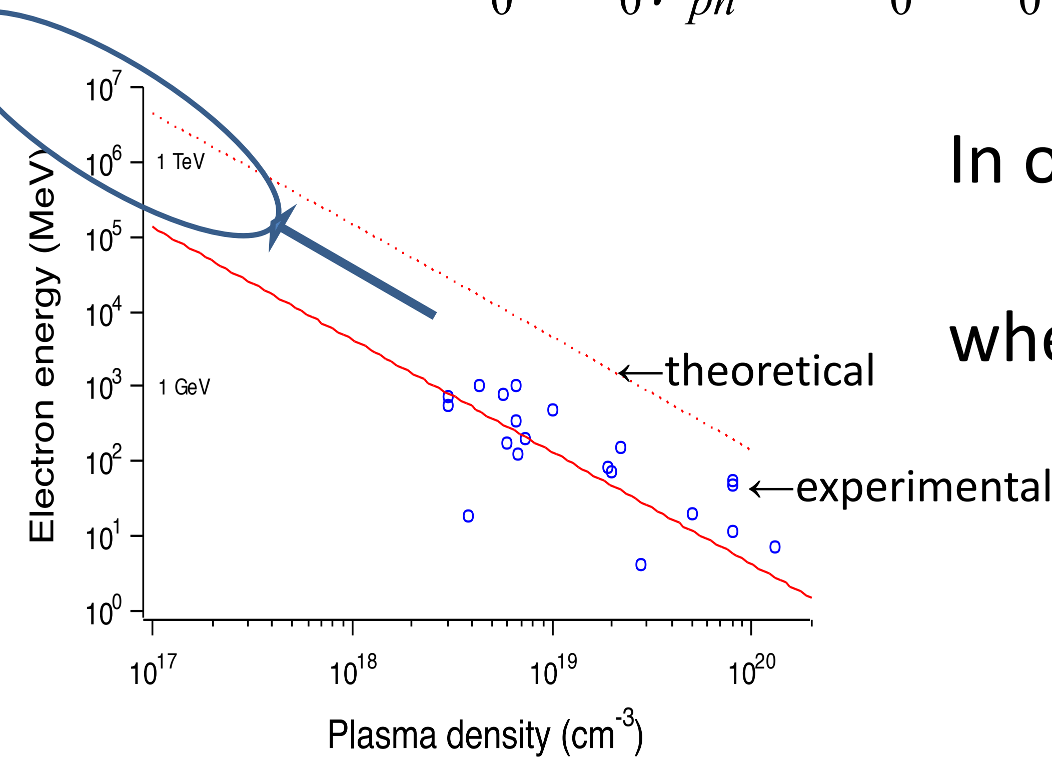

In order to avoid wavebreak,

$$a_0 < \gamma_{ph}^{1/2},$$

where

$$\gamma_{ph} = (n_{cr} / n_e)^{1/2}$$

$n_{cr} = 10^{21}$ (fs photon (laser))

$= 10$ (10^3 s wave in disk)

$n_e = 10^{18}$ (gas)

$= 10^{-2}$ (gas in the jet)

$$L_d = \frac{2}{\pi} \lambda_p a_0^2 \left(\frac{n_{cr}}{n_e} \right),$$

dephasing length

$$L_p = \frac{1}{3\pi} \lambda_p a_0 \left(\frac{n_{cr}}{n_e} \right),$$

pump depletion length

Ultrahigh Energy Cosmic Rays (UHECR)

Fermi mechanism runs out of steam
- beyond 10^{19} eV
- due to synchrotron radiation

Wakefield acceleration
- comes in rescue
- prompt, intense, linear acceleration
- small synchrotron radiation
- radiation damping effects?

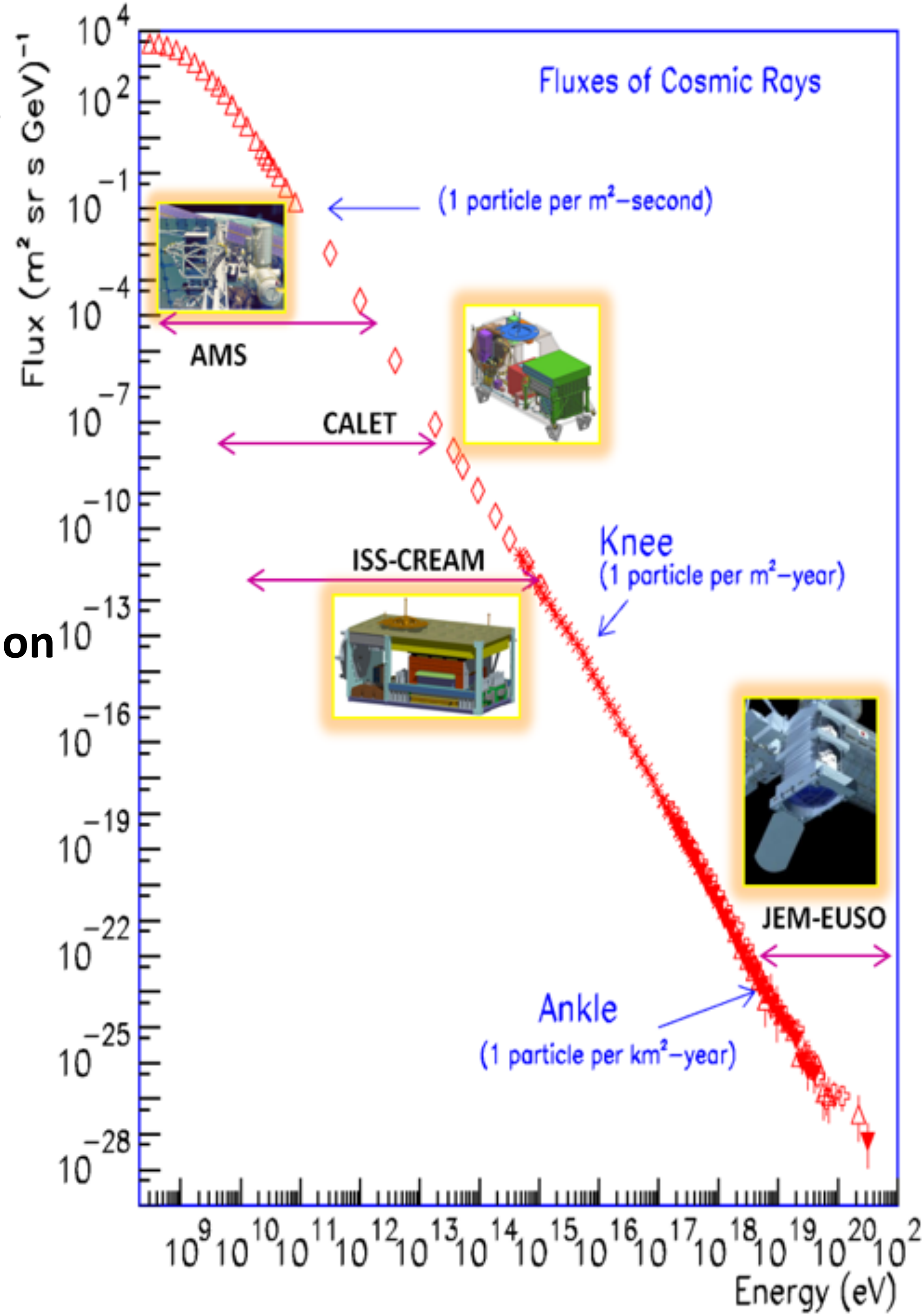

Astrophysical wakefield acceleration: Superintense Alfven Shock in the Blackhole Accretion Disk toward ZeV Cosmic Rays ($a_0 \sim 10^6 - 10^{10}$, large spatial scale)

$a_0 = eE_0 / mc\omega_0 >> 1$: normalized EM wave amplitude

E_0: modest

$\omega_0 = 2\pi c / \lambda$: extremely low

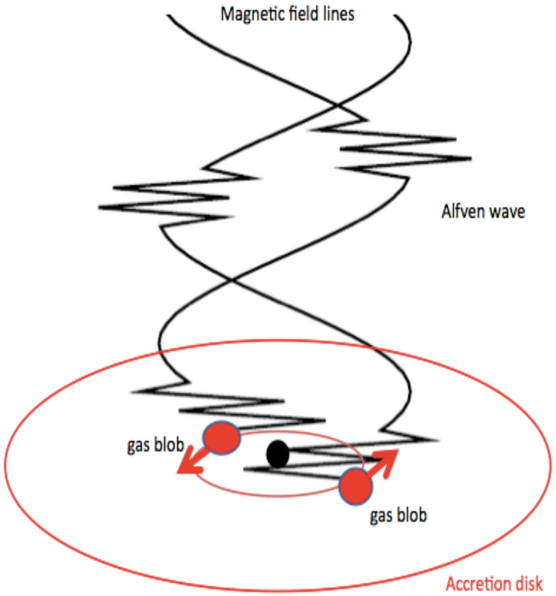

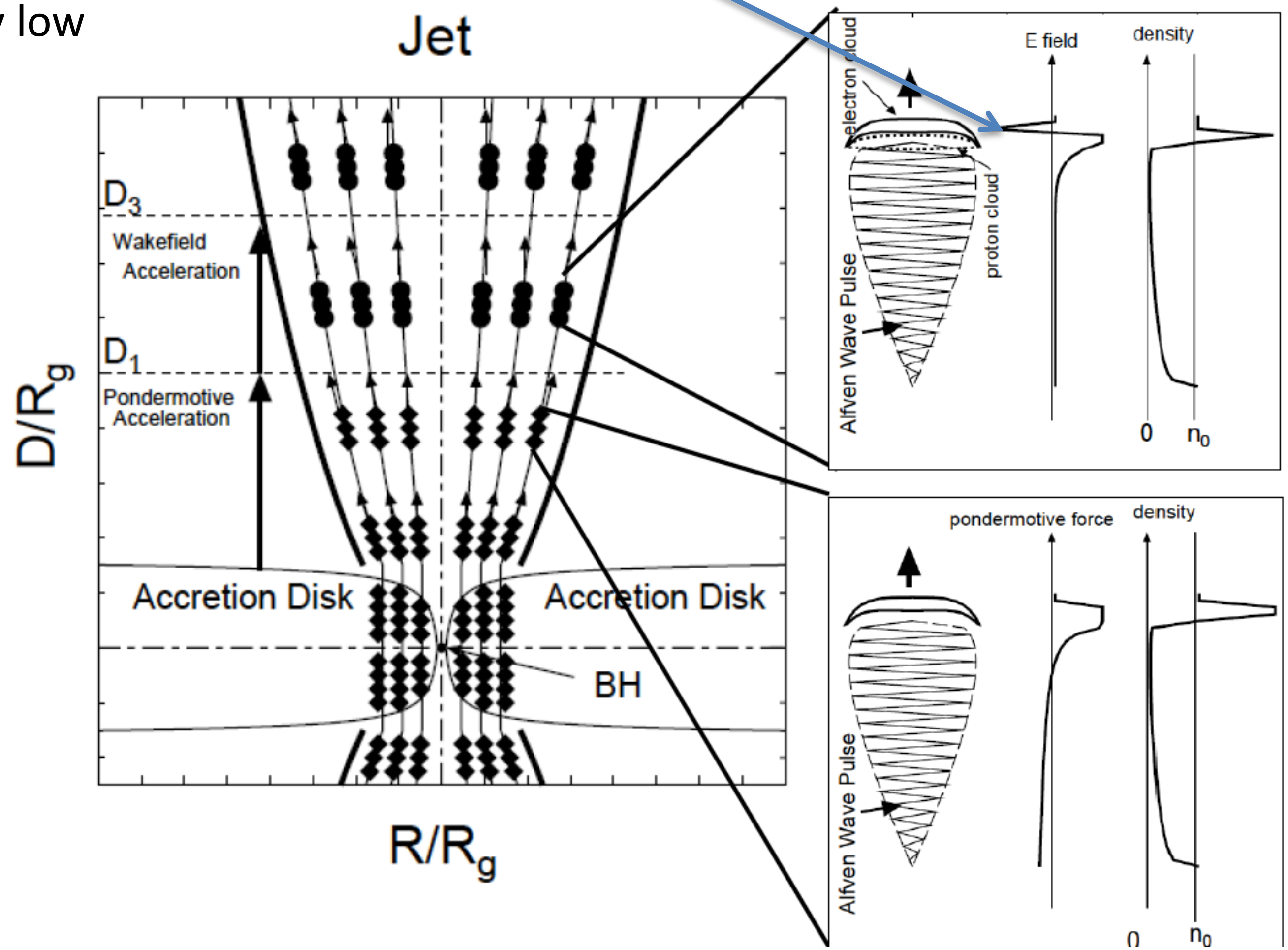

Ebisuzaki and Tajima, Astropart. Phys.(2014)

II. Specific examples ← our theory

0. Blackhole (BH) as an engine of AGN [textbook p.387]

1. Blazar γ-emmission → protons (UHECR); time-structured, coincidental with γ, neutrino

[Canac, et al. 2020;IceCube, Science, 2020]

2. M82 (starburst galaxy) [see refs. inside]

3. Cen A (radio galaxy)

4. NGC 0253 (starburst galaxy)

5. SS 433 (microquasar) [Abeysakara et al., 2018]

[other refs. are also inside of these slides]

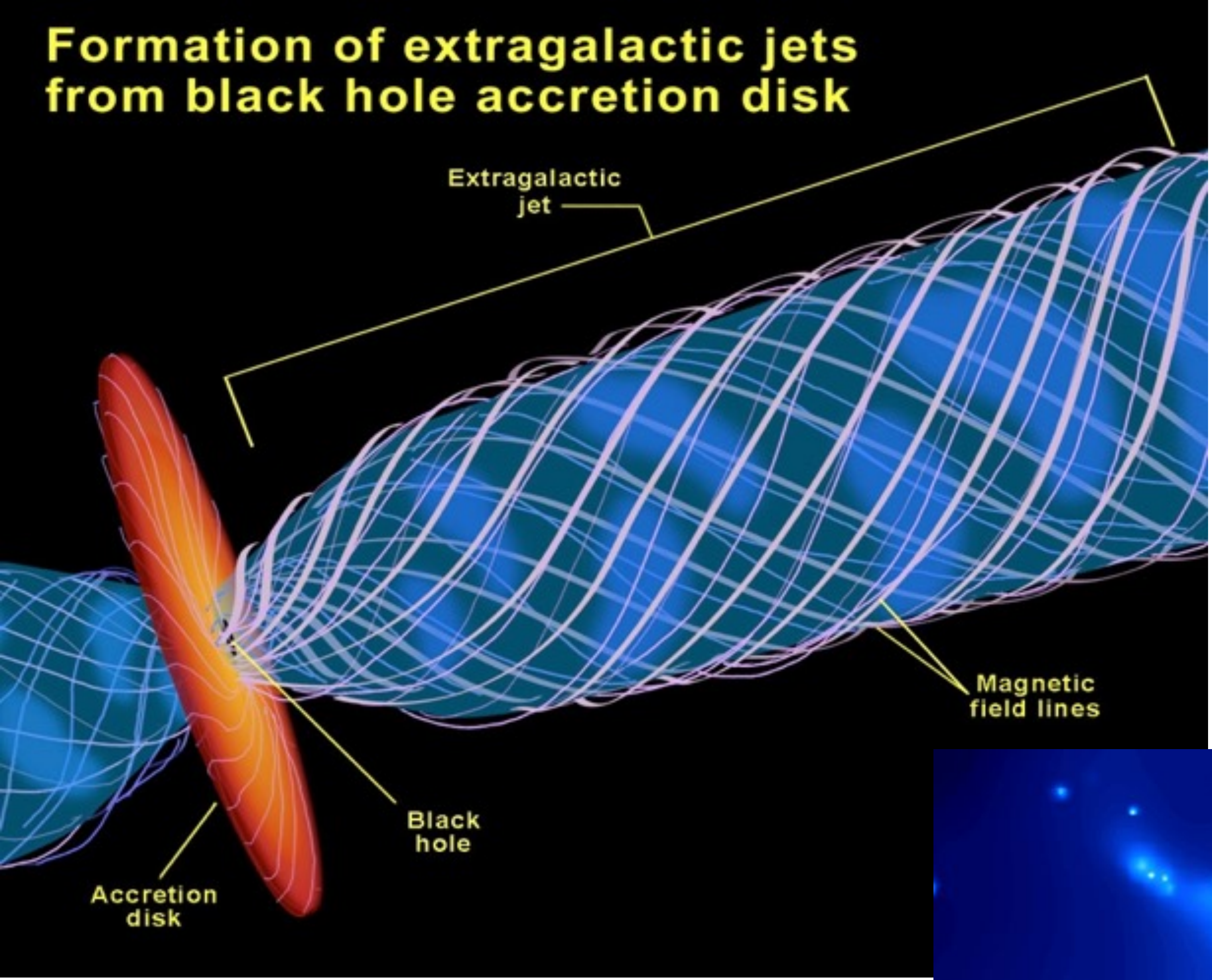

Fermi's **'Stochastic Acceleration'**
(large synchrotron radiation loss)

↓

Coherent wakefield acceleration
(no limitation of the energy)

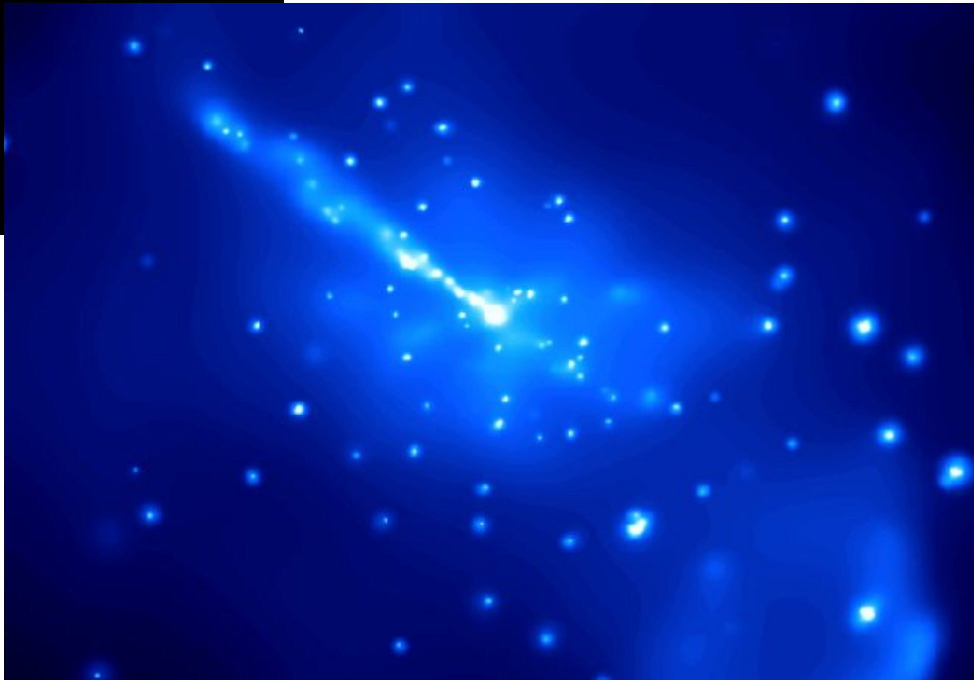

Nature's LWFA : Blazar jets

extreme high energy cosmic rays (~10^{21} eV)

episodic γ-ray bursts observed

consistent with LWFA theory

Ebisuzaki-Tajima (2014)

Halo and jet acceleration in an accretion disk

A Burst of Electromagnetic Disturbance

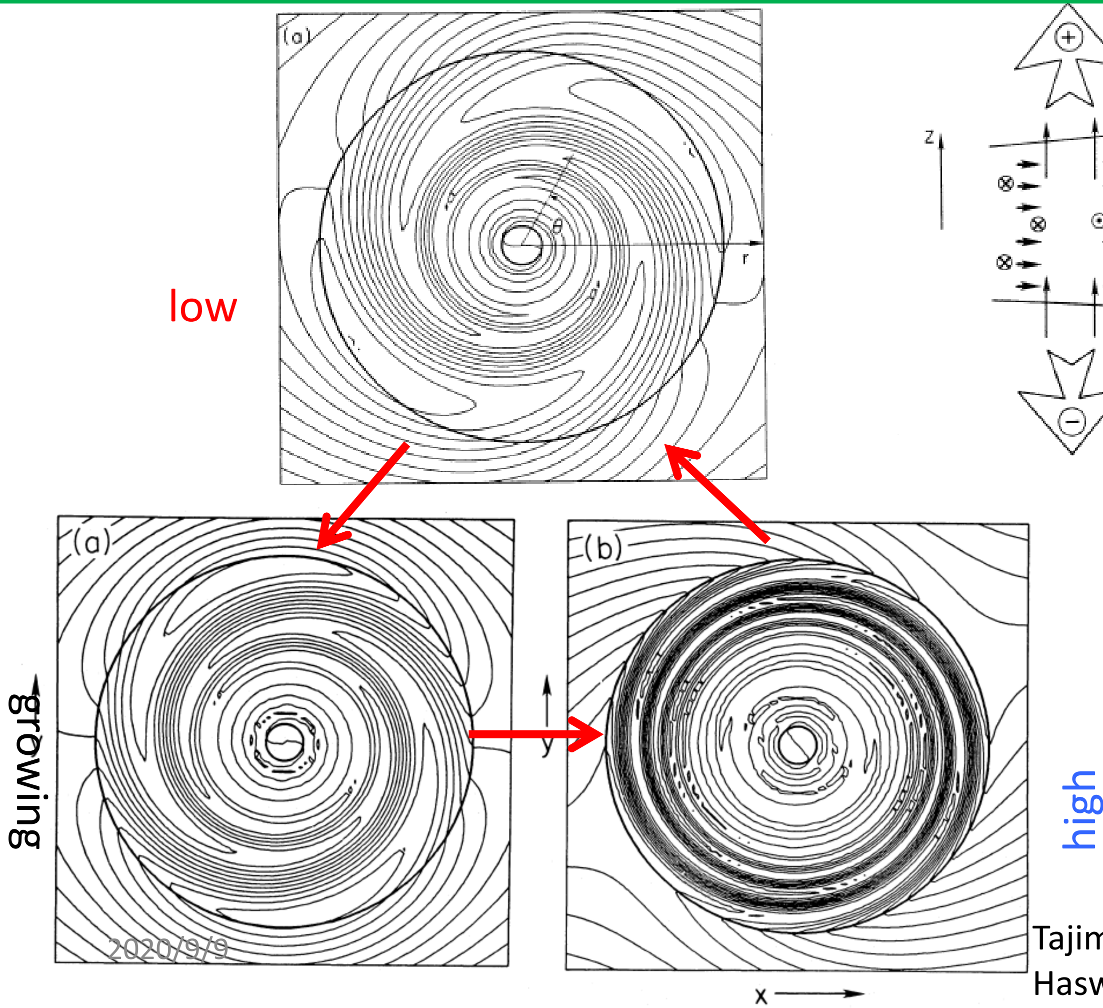

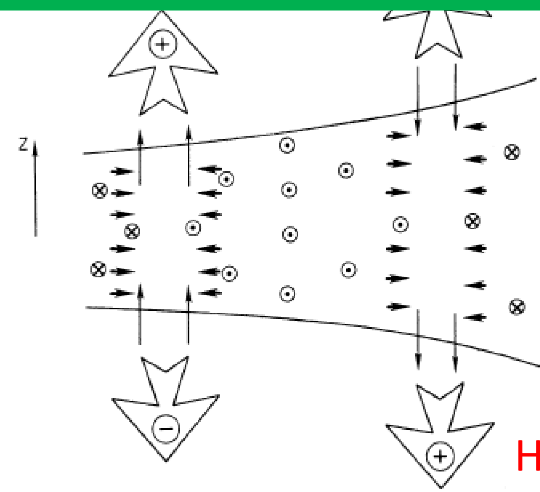

Halo heating and acceleration
→ low energy X, γ, ν

Tajima and Gilden 1987, ApJ 320, 741-745
Haswell, Tajima, and Sakai, 1992, ApJ, 401, 495-507

Anti-correlation of γ flux and spectral index

Blazar: 3C454.3

$M \sim 10^9 M_{Sun}$

Same anti-correlation as
Blazar AO0235+164

The rise time and burst periods
a lot longer (by an order of
magnitude)

Quantitative agreement and
correct scaling with Blazar mass
with (broader sense of) Wakefield theory
(Ebisuzaki/Tajima)
period ~ *M* ; luminosity ~*M*

flux

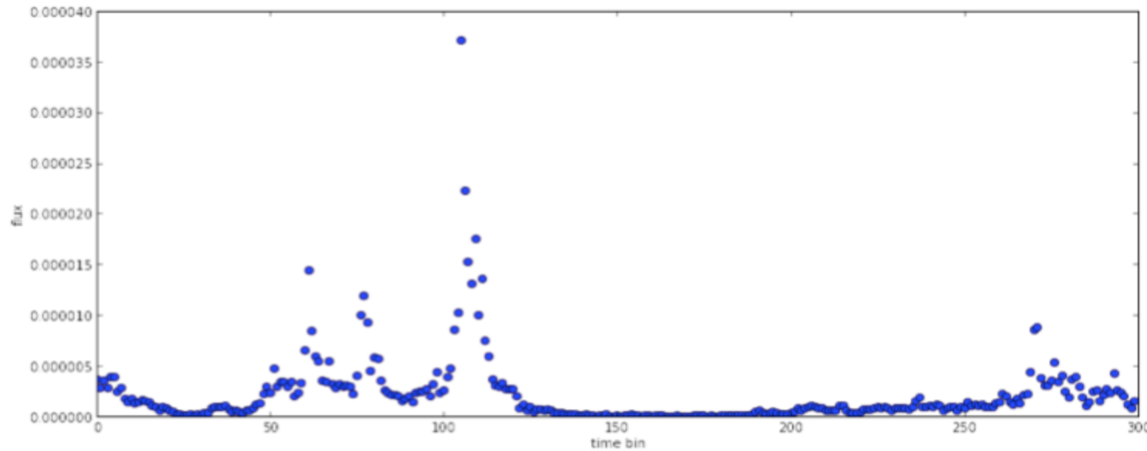

↕ anti-correlate

index

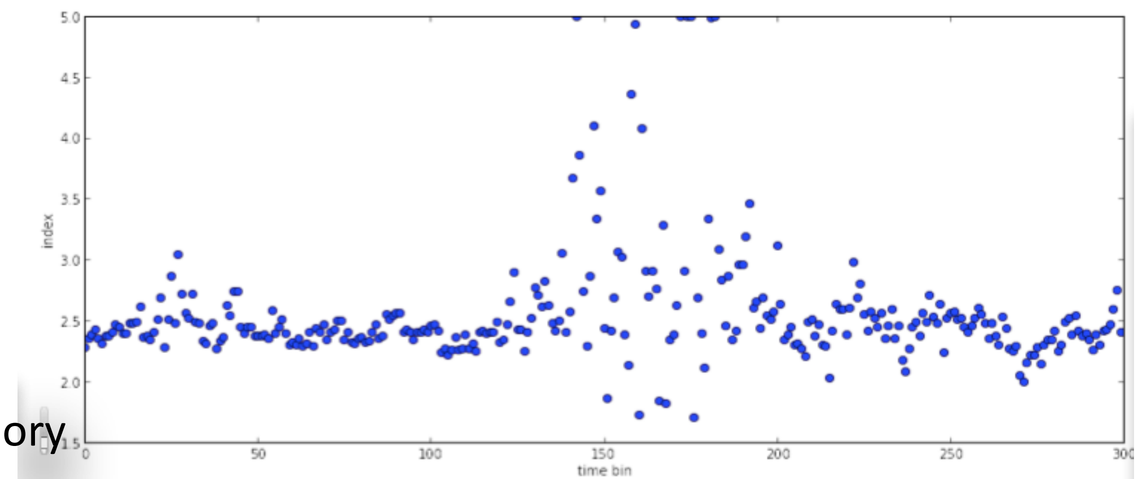

time

N. Canac, et al. MNRAS (2020)

Detected neutrino from **Blazar**

Neutrino: IceCube-170922A / Blazar: TXS 0506+056

Science **361**, 146 (2020) (…,Barwick,…)

Various γ arriavals

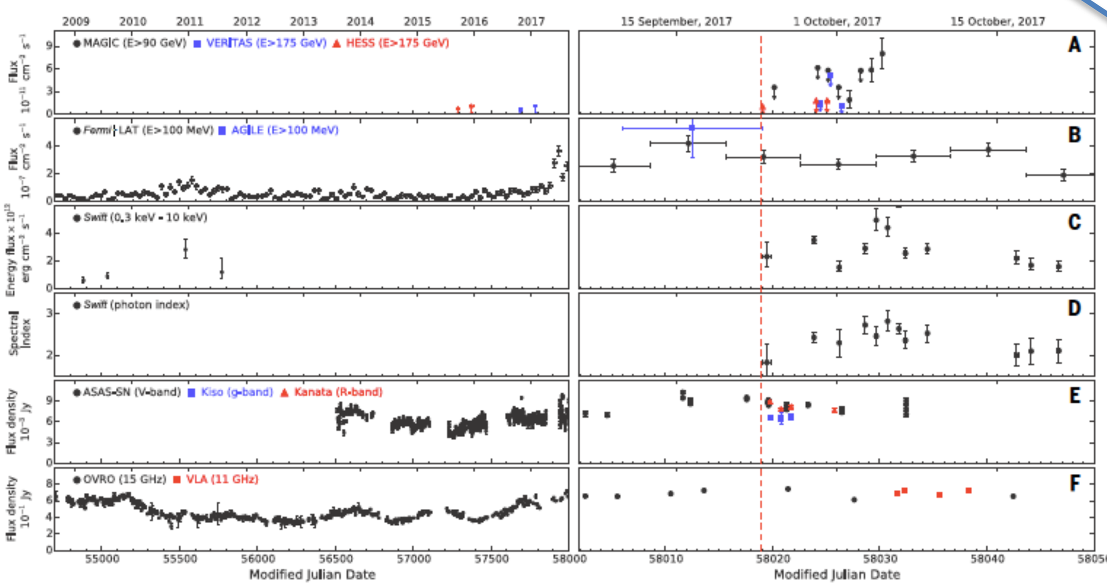

Fig. 3. Time-dependent multiwavelength observations of TXS 0506+056 before and after IceCube-170922A. Significant variability of the electromagnetic emission can be observed in all displayed energy … dashed line marks the detection time of the neutrino IceCube-170922A. The left set of panels shows measurements between MJD 54700 (22 August 2008) and MJD 58002 (6 September 2017). The set of …

10.50 in

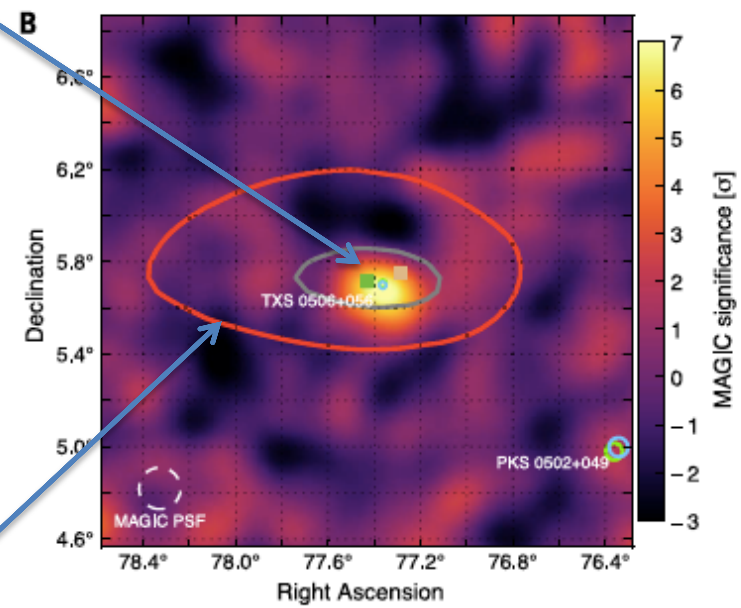

↑
Neutrino arrival

M82: Nearest Starburst Galaxy

M82 X-1: 1000-10000 Ms BH

Just after the collision with M81

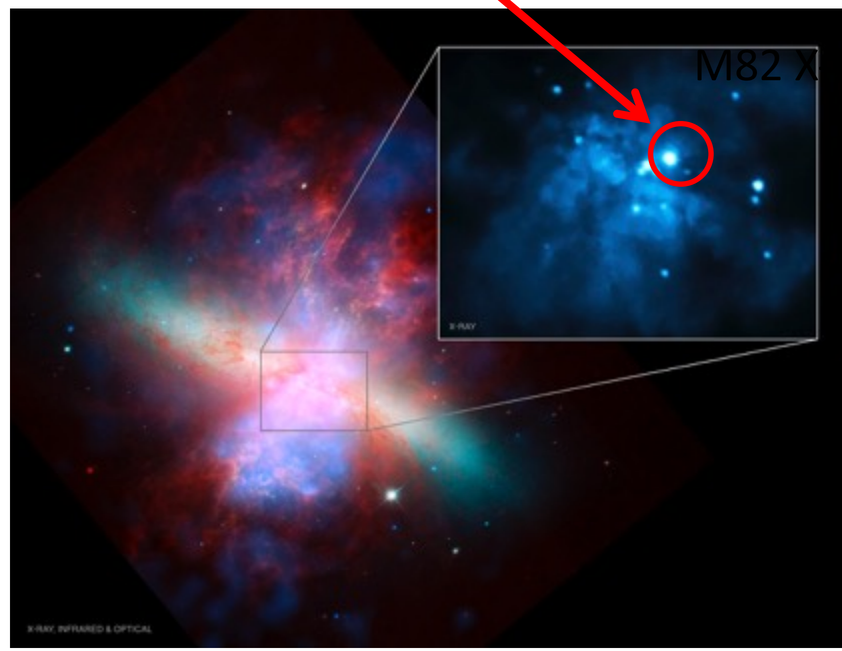

Composite of X-ray, IR, and optical emissions

NASA / CXC / JHU / D. Strickland; optical: NASA / ESA / STScI / AURA/ Hubble Heritage Team; IR: NASA / JPL-Caltech /Univ. of AZ / C. Engelbracht; inset – NASA / CXC / Tsinghua University / H. Feng et al.

TA Hot Spot: UHECRs from M82?

He,Kusenko,Nagataki, , PRD 2016.

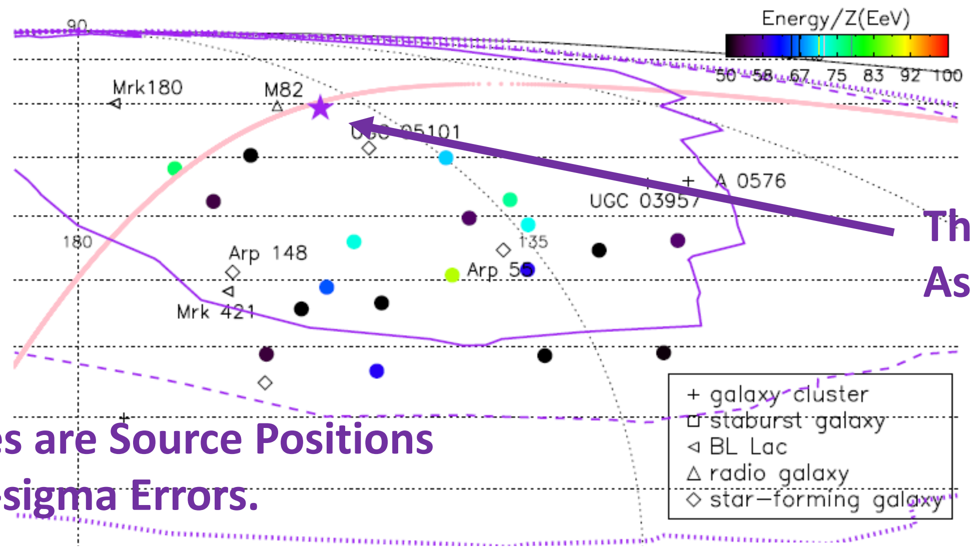

The most likely Source Position
As a Result of Our Analysis.

M82 is very Close from the most likely Source Position!

Purple Lines are Source Positions With 1,2,3-sigma Errors.

Source Name	Source Type	Distance (Mpc)	A_1 (°)	A_2 (°)	$P/P_{\rm bes-fit}$ (%)
best-fit	-	-	$17.4^{+17.0}_{-11.0}$	$9.4^{+3.7}_{-0.3}$	100
M82	starburst galaxy	3.4	17.6	9.6	99.8
UGC 05101	star-forming galaxy	160.2	11.6	9.2	96.9
Mrk 180	blazar	185	19.9	9.3	91.3
UGC 03957	galaxy cluster	150.3	14.9	9.5	67.4
A 0576	galaxy cluster	169.0	17.0	9.4	63.4
Arp 55	star-forming Galaxy	162.7	1.9	9.7	55.3
Arp 148	star-forming Galaxy	143.3	10.5	10.0	41.8
Mrk 421	blazar	134	11.2	9.9	35.6

Arrival Direction Map
(cosmic rays>5×10^{19} eV)

TA

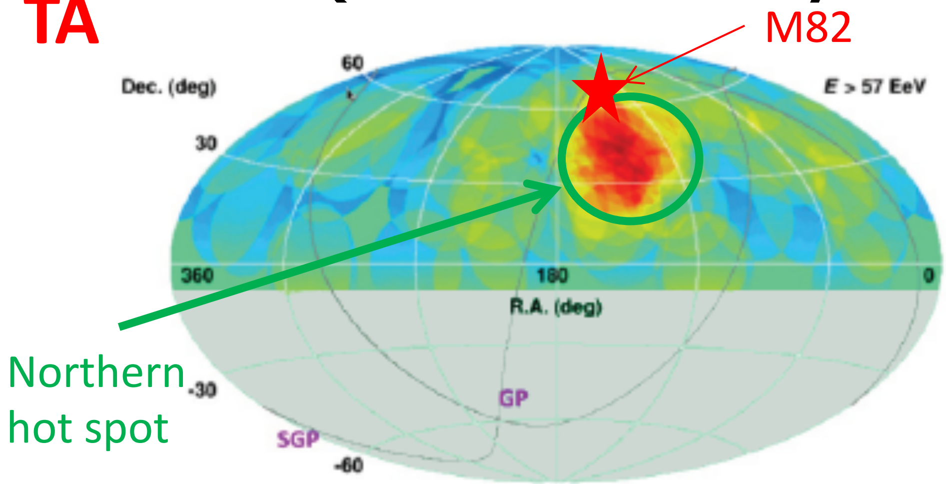

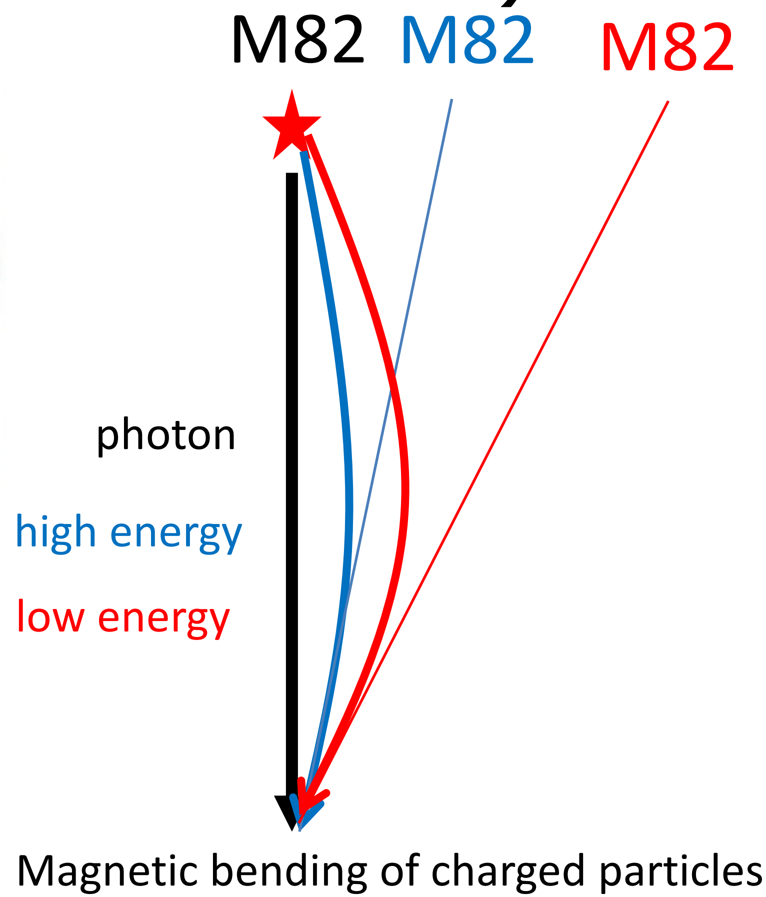

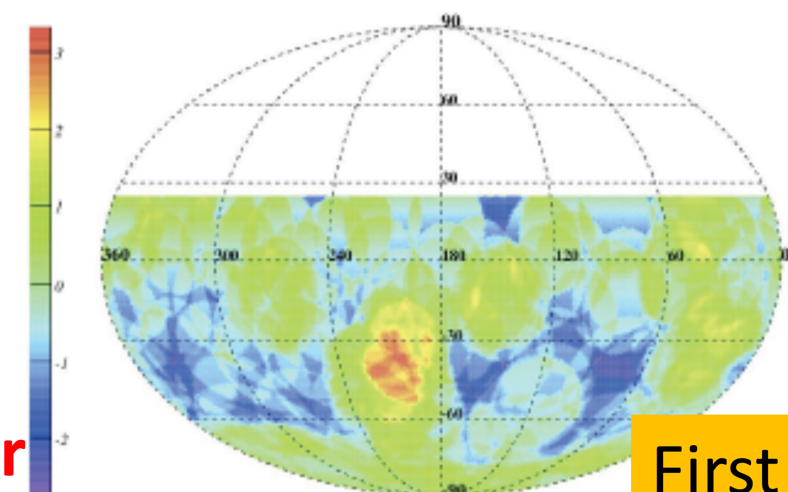

Auger

First Identification of CR sources?

First sign of anisotropy in charged particles

An AGN-like Jet in M82?
X-ray/Radio (flare in 1981)

Xu et al. 2015 ApJ Letters 799, L28

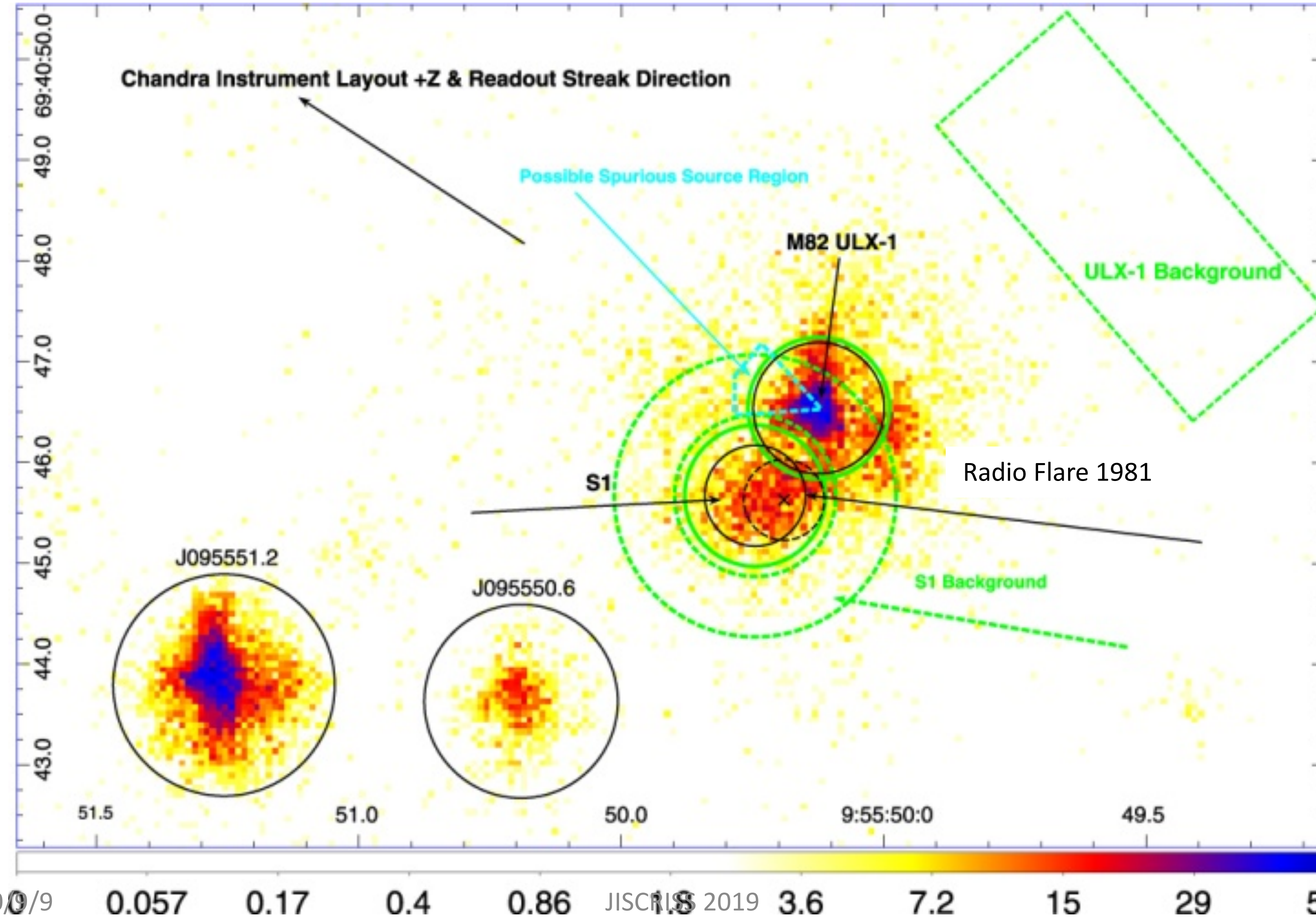

Cen A

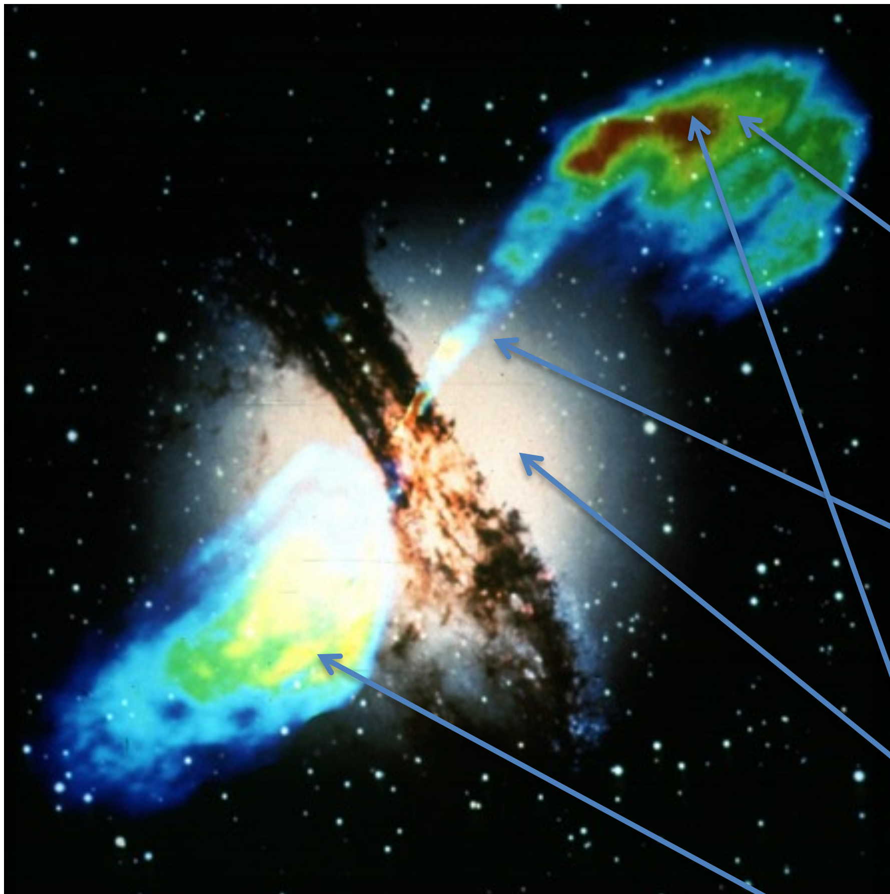

- Distance：3.4Mpc
- Radio Galaxy
  - Nearest
  - Brightest radio source
- Elliptical Galaxy
- Black hole at the center w/ relativistic **jets**, high energy acceleration

Halo emissions

Lobe deceleration of jets

Refs. for Cen A

F. Aharonian; A. G. Akhperjanian; G. Anton; U. Barres de Almeida; A. R. Bazer-Bachi (10 April 2009). "DISCOVERY OF VERY HIGH ENERGY γ-RAY EMISSION FROM CENTAURUS A WITH H.E.S.S.". Astrophysical Journal. 695 (1): L40?L44. --------high energy gamma observation

J. Abraham; P. Abreu; M. Aglietta; C. Aguirre; D. Allard (1 April 2008). "Correlation of the highest-energy cosmic rays with the positions of nearby active galactic nuclei". Astroparticle Physics. 29 (3): 188?204.-------- locale

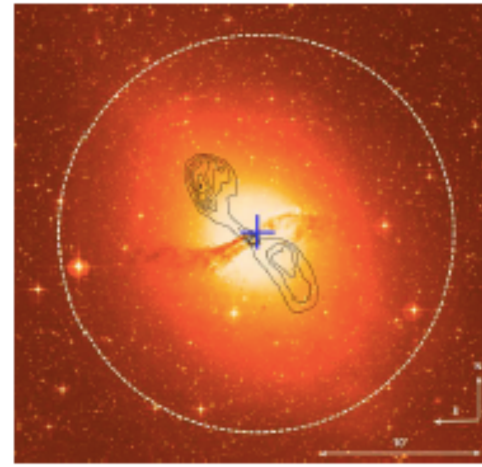

Figure 2. Optical image of Cen A (UK 48 inch Schmidt) overlaid with radio contours (black, VLA, Condon et al. 1996), VHE best fit position with 1σ statistical errors (blue cross), and VHE extension upper limit (white dashed circle, 95% confidence level).

The differential photon spectrum of the source is shown in Figure 3.[36] A fit of a power-law function $dN/dE = \Phi_0 \cdot (E/1\,\mathrm{TeV})^{-\Gamma}$ to the data is a statistically good description ($\chi^2/\mathrm{dof} = 2.76/4$) with normalization $\Phi_0 = (2.45 \pm 0.52_{\mathrm{stat}} \pm$

[36] To derive the energy spectrum, a looser cut on the distance to the source is used ($\theta^2 < 0.03\,\mathrm{deg}^2$) to increase the number of photons (the standard cut is $\theta^2 < 0.015\,\mathrm{deg}^2$).

No. 1, 2009 DISCOVERY OF VHE γ-RAY EMI

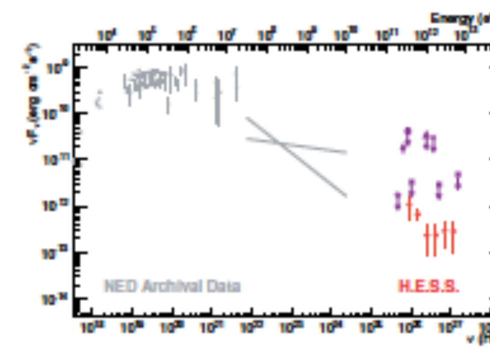

Figure 4. SED of Cen A. Shown are the VHE spectrum as measured by H.E.S.S. (red filled circles), previous upper limits and tentative detections in the VHE regime (purple markers; Grindlay et al. 1975: open diamond; Carramiñana et al. 1990: open cross; Allen et al. 1993: filled circle; Rowell et al. 1999: open triangle; Aharonian et al. 2005: open circle; Kabuki et al. 2007: filled squares), EGRET measurements in the GeV regime (Sreekumar et al. 1999: gray bow tie), and data from the NASA Extragalactic Database (NED; gray filled circles).

NGC 0253: Starburst galaxy

Gamma emission:

Abdo et al. 2010, Detection of gamma-ray emission from the starburst galaxies M82 and NGC253 with the Large Area Telescope on FERMI, Astrophys. J. Letters, L152-L157.

X-ray source found:

R. Barnard, 2010, In-depth studies of NGC253 ULXs with XMM-Newton: remarkable variability in ULX1, and evidence for extended coronae, Mon. Not. Roy. Soc, 404, 42-47.

NGC253

n from our survey of X-ray sources in NGC 253 (Barnard et al. 2008b). For
ned by the source detection routine; these have uncertainties of ∼2 arcsec.
n and MOS detectors. Next, we give the details of the best-fitting spectral
T) and photon index (Γ), along with the corresponding χ^2/d.o.f. and 0.3–
heses indicate 90 per cent confidence limits on the final digit.

OS	$N_H/10^{21}$ atom cm^{-2}	kT/keV	Γ	χ^2/d.o.f.	$L/10^{39}$
90	2.00(2)	0.73(5)	2.14(4)	347/323	2.90(12)
14	2.9(2)	0.98(6)	1.94(5)	374/374	4.10(19)
56	6.0(11)	0.94(8)	3.4(5)	84/76	2.4(4)

top of
QPOs
er-law
08 X-1
).
udy of
vations
power
C 1313
others
l upper
hat the

y spec-
power
ons on
dstone,
xcess',
1 com-
andard
by the
006).
Newton
EPIC
and a
inner
excess
disc +
wever,

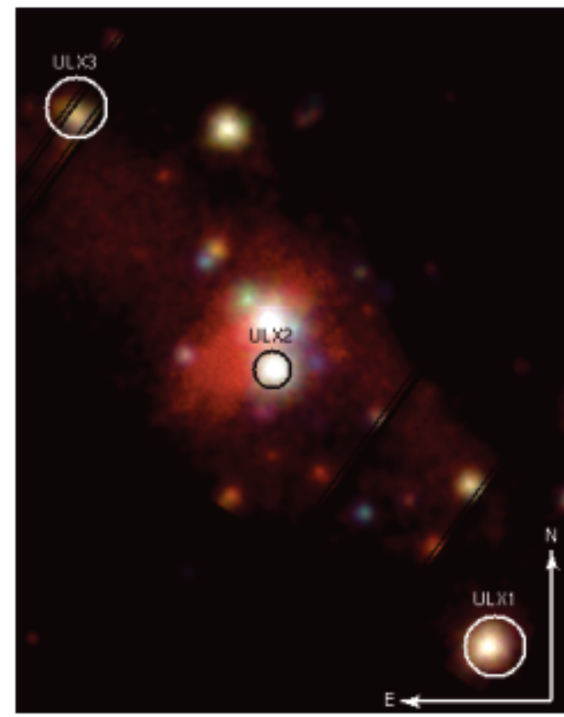

Figure 1. Detail of a three colour pn + MOS image of NGC 253 showing ULX1, ULX2 and ULX3. Red represents 0.3–2.0 keV, green represents 2.0–3.0 keV, and blue represents 4.0–10 keV. The image is log-scaled, and the source extraction regions for the ULXs are labelled.

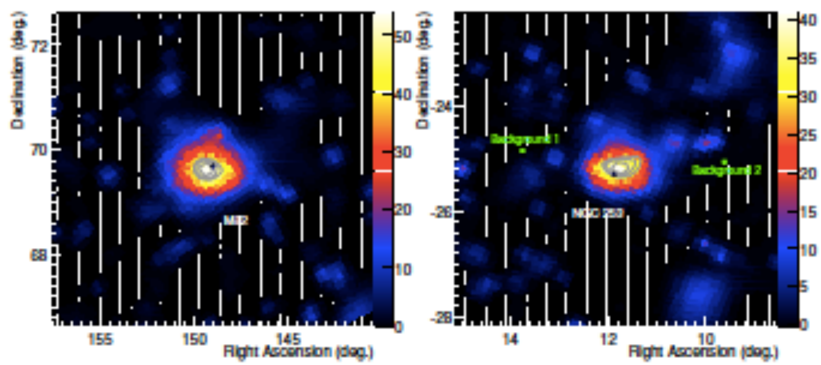

Figure 1. Test statistic maps obtained from photons above 200 MeV showing the celestial regions (6° by 6°) around M82 and NGC 253. Aside from the source associated with each galaxy, all other *Fermi*-detected sources within a 10° radius of the best-fit position have been included in the background model as well as components describing the diffuse Galactic and isotropic γ-ray emissions. Black triangles denote the positions of M82 and NGC 253 at optical wavelengths; gray

SS 433: Microquasar

Gammaray energy ~ 10TeV Abeysekara, et al. (2018)

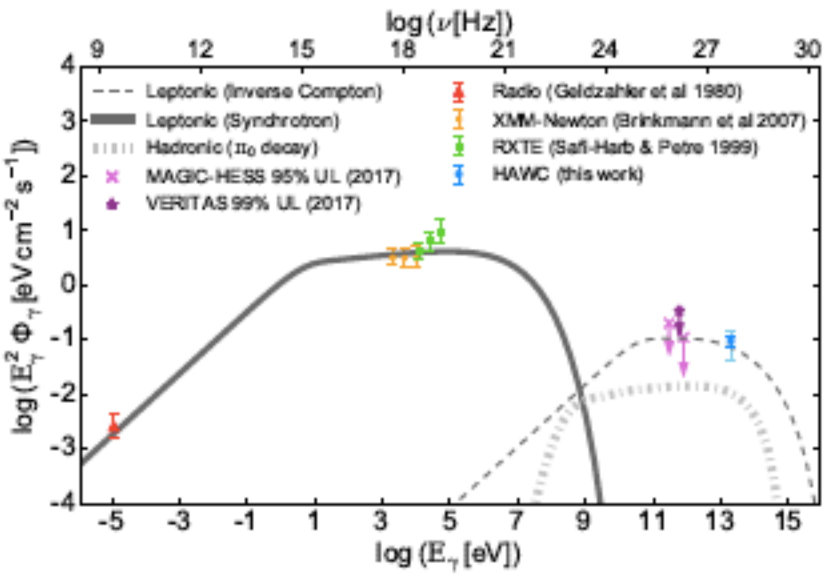

Figure 2: **Broadband spectral energy distribution of the eastern emission region.** The data include radio, soft X-ray, hard X-ray, and VHE γ-ray upper limits, and HAWC observations of e1. Error bars indicate 1σ uncertainties, with the thick (thin) errors on the HAWC flux indicating statistical (systematic) uncertainties and arrows indicating flux upper limits. The multiwavelength spectrum produced by electrons assumes a single electron

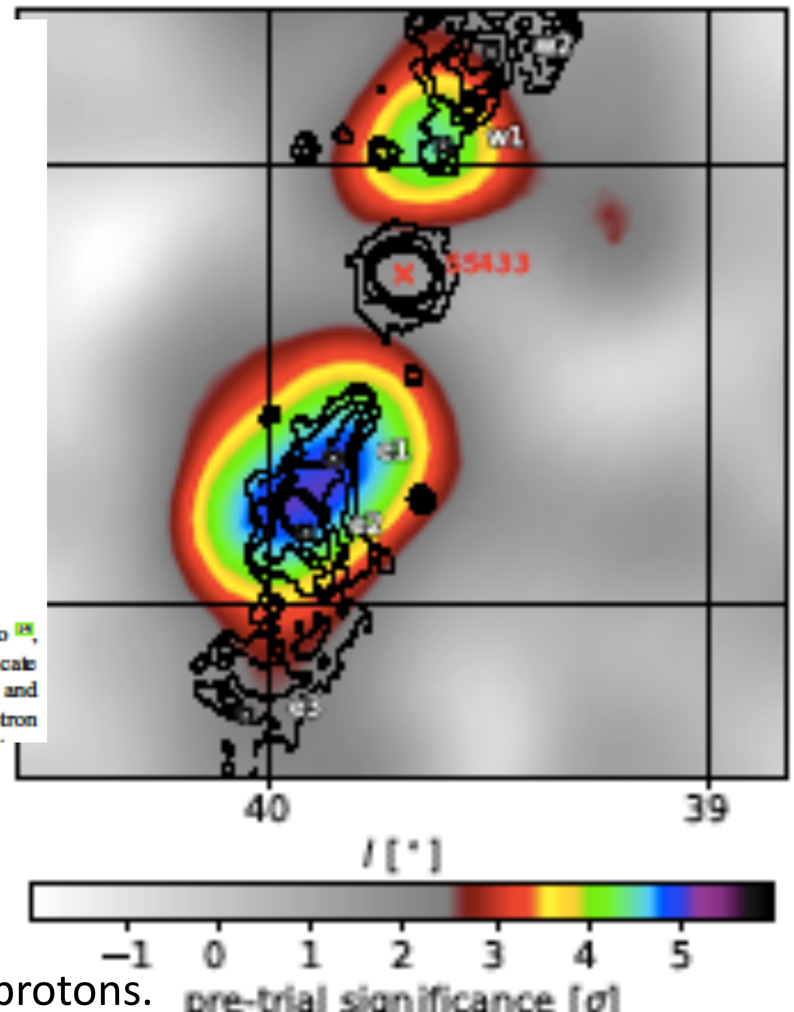

[Wakefield proton theory:
could go as high as 3×10^{19} eV]: Can we observe?
galactic center's dense plasma and B might affect protons.

SS433 precession jets

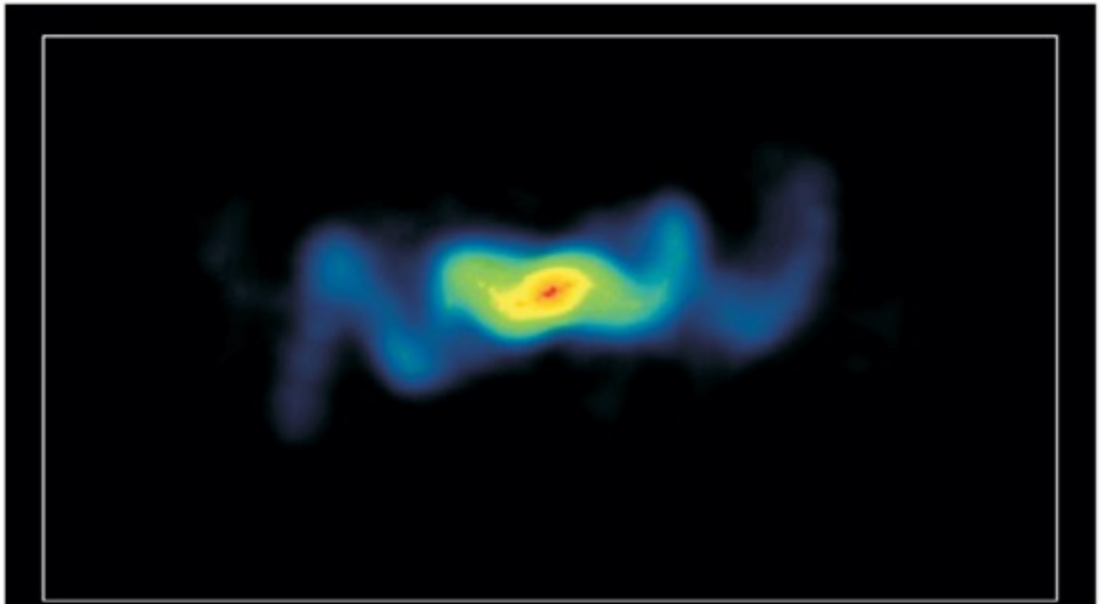

III. Generalized jets

[see the memo written by Ebisuzaki et al.(2020) on
the general index parameter *p* ~ (0, 1)
for the jet expansion geometry .
You could pick different numbers
for *p* such as 0.3, 0.7.
0.5 was taken in Ebisuzaki et al. (2014)]

Power index *p*, characterizing the jet confinement

Wakefield acceleration in accreting blackhole systems -----

Pependence on power index p

Toshikazu Ebisuzaki[1] and Toshiki Tajima[2]
[1]RIKEN
[2]University of California Irvine

Accreting gas forms a disk around a blackhole.[154] In the accretion disk, gas slowly inward while orbiting in a circular orbit around the blackhole. The velocity and orbital angular velocity are given as follows:

$$v_\varphi = \left(\frac{GM_{\rm BH}}{R}\right)^{\frac{1}{2}} = \frac{c}{\sqrt{6}}\frac{1}{r^{\frac{1}{2}}} \qquad \#(\mathrm{VI.\,1})$$

$$\Omega = \left(\frac{GM_{\rm BH}}{R^3}\right)^{1/2} = \frac{c}{\sqrt{6}R_0}\frac{1}{mr^{1/2}} \qquad \#(\mathrm{VI.\,2})$$

Next, we assume as

$$\gamma = a_0 \qquad \#(\mathrm{VI.\,48})$$

within the jet, a_0 can be calculated, assuming that the wave intensity within the jet is conserved, i.e., the flux $\Phi_{\rm w,jet}$ is inversely proportional to the cross-sectional area πb^2 of the jet.

$$a_0(D) = a_0(D = R_0)\left(\frac{b(D)}{R_0 m}\right)^{-1} \qquad \#(\mathrm{VI.\,49})$$

where D is the distance from the bottom of the jet, and $b(D)$ is the radius of the jet, which is assumed to $b(0) = 3R_g = R_0 m$. In addition, Figure 2 shows the ratio ω_c'/ω of the cyclotron frequency to the wave frequency and that of plasma frequency ω_p'/ω

are plotted against the distance $D/(R_0 m)$ from the bottom of the jet for the typical cases ($\Gamma = 10$, $\alpha = 0.1$, $\xi = 10^{-2}$, $\dot{m} = 0.1$ for $m = 1, 10^4, 10^8$). Here we assume that

$$b(D) = R_0 m (D/R_0 m)^p \qquad \#(\mathrm{VI.\,50})$$

The power law index p is in the range of 0 to 1. According to the observation of the jet of M87, the closest active galactic nuclei M87[155] and other AGN jet observation, $p \sim 0.5$.[156] Now, we get

$$a_0(D) = \frac{e}{36 m_e c}\sqrt{\frac{R_0}{\pi \epsilon^3 \kappa_T}}\,\alpha^{3/4}\dot{m}^{3/2}m^{1/2}\left(\frac{D}{R_0 m}\right)^{-p} \qquad \#(\mathrm{VI.\,51})$$

Substituting equations 47, 48, and 51 into equation 46, we attain

$$\omega_c' = \frac{144 c\pi}{R_0}\left(\frac{\epsilon^3}{3\sqrt{6}}\right)^{1/2}\frac{1}{\alpha^{3/4}\dot{m}^{3/2}m}\left(\frac{D}{R_0 m}\right)^{p-1} \qquad \#(\mathrm{VI.\,52})$$

etc. etc. (see the sent note)

IV. Emerging new view of the Universe

Conventional view:

Quiet, nearly steady, slow-evolving Universe

……..

New view:

Violent, active, fast-evolving Universe

……….